

LUCIFER@LBT view of star-forming galaxies in the cluster 7C 1756+6520 at $z \sim 1.4$

Laura Magrini¹, Veronica Sommariva¹, Giovanni Cresci¹, Eleonora Sani¹,
Audrey Galametz², Filippo Mannucci¹, Vasiliki Petropoulou³, Marco Fumana⁴

¹ *INAF - Osservatorio Astrofisico di Arcetri, Largo E. Fermi 5, I-50125, Firenze, Italy*

² *INAF Osservatorio Astronomico di Roma, Via Frascati 33, I-00040, Monteporzio (Roma), Italy*

³ *Instituto de Astrofísica de Andalucía-C.S.I.C., Glorieta de la Astronomía, E-18008 Granada, Spain*

⁴ *INAF - Istituto di Astrofisica Spaziale e Fisica cosmica, Milano, Italy*

Accepted ?. Received ?; in original form ?

ABSTRACT

Galaxy clusters are key places to study the contribution of *nature* (i.e. mass, morphology) and *nurture* (i.e. environment) in the formation and evolution of galaxies. Recently, a number of clusters at $z > 1$, i.e. corresponding to the first epochs of the cluster formation, has been discovered and confirmed spectroscopically. We present new observations obtained with the LUCIFER spectrograph at Large Binocular Telescope (LBT) of a sample of star-forming galaxies associated with a large scale structure around the radio galaxy 7C1756+6520 at $z = 1.42$. Combining our spectroscopic data and the literature photometric data, we derived some of the properties of these galaxies: star formation rate, metallicity and stellar mass. With the aim of analyzing the effect of the cluster environment on galaxy evolution, we have located the galaxies in the plane of the so-called Fundamental Metallicity Relation (FMR), which is known not to evolve with redshift up to $z = 2.5$ for field galaxies, but it is still unexplored in rich environments at low and high redshift. We found that the properties of the galaxies in the cluster 7C 1756+6520 are compatible with the FMR which suggests that the effect of the environment on galaxy metallicity at this early epoch of cluster formation is marginal. As a side study, we also report the spectroscopic analysis of a bright AGN, belonging to the cluster, which shows a significant outflow of gas.

Key words: galaxies: clusters: individual: 7C 1756+6520 – galaxies: abundances – galaxies: evolution – galaxies: star formation

1 INTRODUCTION

Located at nodes of the cosmic web, clusters of galaxies are the largest collapsed structures in the Universe with total masses up to $10^{15} M_{\odot}$. Over 80% of their mass resides in the form of dark matter, whereas the remaining mass is composed of baryons, most of which (about 85%) is a diffuse, hot $T > 10^7$ K plasma, the intracluster medium (ICM) (e.g., Arnaud 2009). It is known that galaxy evolution is closely linked to the formation of structures in the Universe. In the Local Universe, both galaxy morphology and star formation history have been found to correlate with the environment, with passive early-type galaxies dominating the dense regions (e.g., Dressler et al. 1980; Finn et al. 2005). This points towards a differential evolution between isolated and cluster galaxies (e.g., Poggianti et al. 2006; Bolzonella et al. 2010) which results in a strong environmental dependence of galaxy properties in the local Universe (e.g., di Serego

Alighieri et al. 2005; Chung et al. 2009; Petropoulou et al. 2012).

In this framework, many questions have risen during the last decades about the effect of the environment in galaxy evolution, for example: when were the visible parts of galaxies assembled, when were the stars formed, and how did this depend on the environment? Is it *nature* (i.e. mass, morphology) and/or *nurture* (i.e. environment) that governs the evolution of a galaxy? which is the origin of the morphological segregation? By studying different stages of their evolution, galaxy clusters are among the best tools to seek answers to these questions.

Most of the recent studies have been devoted to clusters at $z < 1$. From these studies it has been found that the environmental dependence of galaxy properties is already strong at $z = 1$, with red galaxies being the dominant population (e.g., Blakeslee et al. 2003; Nakata et al. 2005; Lidman et al. 2008). Due to the smaller number of galaxy clusters confirmed at $z > 1$, it has been challenging until now to repro-

duce these studies at higher redshift. However, the number of spectroscopically confirmed clusters at $z > 1$ has significantly increased in the last few years thanks to new efficient selection techniques e.g. wide surveys in the mid-infrared (Eisenhardt et al. 2008; Wilson et al. 2009; Papovich 2008), deep X-rays observations of the ICM (Lidman et al. 2008; Hilton et al. 2009) or targeted studies in the field of radio galaxies (Galamez et al. 2009, 2010B, and references therein). This last selection technique has permitted the discovery of a galaxy cluster associated with 7C1756+6520 — a radio galaxy at $z=1.42$ — on which this paper is focussed (see Section 2). To date, the two highest redshift (spectroscopically confirmed) galaxy clusters, discovered using mid-infrared selection techniques, were found at $z=1.62$ (Papovich et al. 2010; Tanaka et al. 2010) and $z=2$ (Gobat et al. 2011). The increasing number of proto-clusters (associated with high-redshift radio galaxies) at $z>2$ and up to $z\sim 6$ (among others, Venemans et al. 2007; Hatch et al. 2011; Kuiper et al. 2011) opens even broader perspectives for the study of galaxy properties dependence with environment and cosmic time.

The metal content of galaxies is an important tracer of their evolutionary stage. In the Local Universe, it is now well established (Lequeux et al. 1979) that gas-phase metallicity and stellar mass of galaxies are tightly related in a mass-metallicity relation, with more massive galaxies being also more metal rich (see, for example, Tremonti et al. 2004). Several studies have demonstrated that this relation evolves with redshift, with metallicity decreasing with redshift at a given mass (e.g., Erb et al. 2006; Maiolino et al. 2008; Mannucci et al. 2009). A similar relation was observed also between stellar metallicities and stellar masses (Sommariva et al. 2011). However, a more fundamental relation seems to be in place: Mannucci et al. (2010) found that metallicity depends not only on mass, but also on star formation rate (SFR), with more star-forming galaxies, showing lower metallicities at a given stellar mass. At $z=0$, local galaxies define a surface in the mass-SFR-metallicity space (see Fig. 2 in Mannucci et al. 2010), called the Fundamental Metallicity Relation (FMR), in which the spread of the metallicity around this relation is lower than in the *classical* Mass-Metallicity (Z) Relation (MZR) (0.05 dex vs 0.10 dex). In contrast to the MZR, *the FMR does not evolve with redshift*, i.e., all the observed galaxies up to $z= 2.5$ are found to follow the same local relation (see, e.g., Cresci et al 2012; Mannucci et al. 2011, for an extension towards low masses). The origin of the FMR is not still completely clear, but it is probably due to a combination of several effects: infall of pristine gas, outflow of enriched material, different efficiencies of star formation for different masses (*chemical downsizing*). Its existence and the lack of evolution up to $z= 2.5$, $\sim 80\%$ of the Hubble time, means that this is really a fundamental relation tightly linked to the *nature* of the processes of galaxy formation (see, e.g., Davé et al. 2011; Campisi et al. 2011; Dayal et al. 2012).

The aim of the present work is to derive, for the first time, gas-phase metallicities, stellar masses, and SFRs of a sample of star-forming galaxies belonging to one of the farther spectroscopically confirmed clusters of galaxies, at $z\sim 1.4$. This will allow us to study, for the first time, the FMR in a rich environment at high redshift analyzing if the cluster membership alters the location of galaxies along the

FMR plane. In particular, different effects on the FMR in dense environments are expected if the dominant processes are the infall or the outflow: for example, since the ICM is metal rich, an infall of already enriched gas could have an effect on the FMR radically different than an infall of pristine gas.

In addition, the mask design has allowed us to include the observations of an active galactic nucleus (AGN) (belonging to the cluster, for which we could analyze the line profiles identifying the origin of the blue wings in its emission lines). The paper is structured as follows: in Sec.2 we present the main characteristics of the cluster 7C 1756+6520 and its literature data. In Sec.3 we describe the observations and the selection of the targets to be observed spectroscopically, and in Sec.3.1 the spectroscopic observations and how the parameters of galaxies (stellar mass, SFR, and metallicity) are derived (Sec.4). In Sec.5 we discuss the FMR for the cluster galaxies, and in Sec.6 we present the spectroscopic analysis of an AGN belonging to the cluster. Finally, in Sec.7 we give our conclusions.

2 A CLUSTER AT $Z\sim 1.42$ AROUND 7C 1756+6520

Galamez et al. (2009) (hereafter, G09) made use of the well known BzK selection technique (Daddi et al. 2004) to isolate $z>1.4$ galaxy candidates in the surroundings of 7C 1756+6520, a radio galaxy at $z=1.42$ and found an over-density of $z=1.4$ candidates in this field. The existence of this large scale structure of galaxies was then confirmed by Galamez et al. (2010) (hereafter, G10) through optical Keck/DEIMOS spectroscopy. They assigned a redshift of $z= 1.4156$ to the radio galaxy, and about twenty galaxies with spectroscopic redshifts consistent with the redshift of 7C 1756+6520 were confirmed. They found that seven of these galaxies have velocity offsets $v<1000 \text{ km s}^{-1}$ relative to the redshift of the radio galaxy and are within ~ 2 Mpc from the radio galaxy, forming a first sub-structure located around the radio galaxy. In addition they found a second sub-structure, located at the East of the radio galaxy, with a redshift of $z\sim 1.44$.

3 OBSERVATIONS

The observations presented here were carried out with the Large Binocular Telescope (LBT), located on Mount Graham, Arizona (Hill et al. 2006), using the spectrograph LUCIFER (Ageorges et al. 2010; Seifert et al. 2010). The NIR spectrograph LUCIFER is mounted on the bent Gregorian focus of the left primary mirror with a wavelength coverage from 0.85 to 2.4 μm (zJHK bands) in imaging, long-slit, and multiobject spectroscopy modes.

The mask design was done starting with the list of star-forming galaxies and with the B-band image of G10. To maximize the number of galaxies to be observed with a single LUCIFER mask, we centered the mask at R.A. 17:57:13.03, Dec. 65:19:13.5 (J2000.0), with a rotation angle respect to the North of 250 degrees. We selected seven star-forming galaxies, identified by G10 from the optical spectroscopy thanks to their intense [OII] 3727 Å emission line, and two

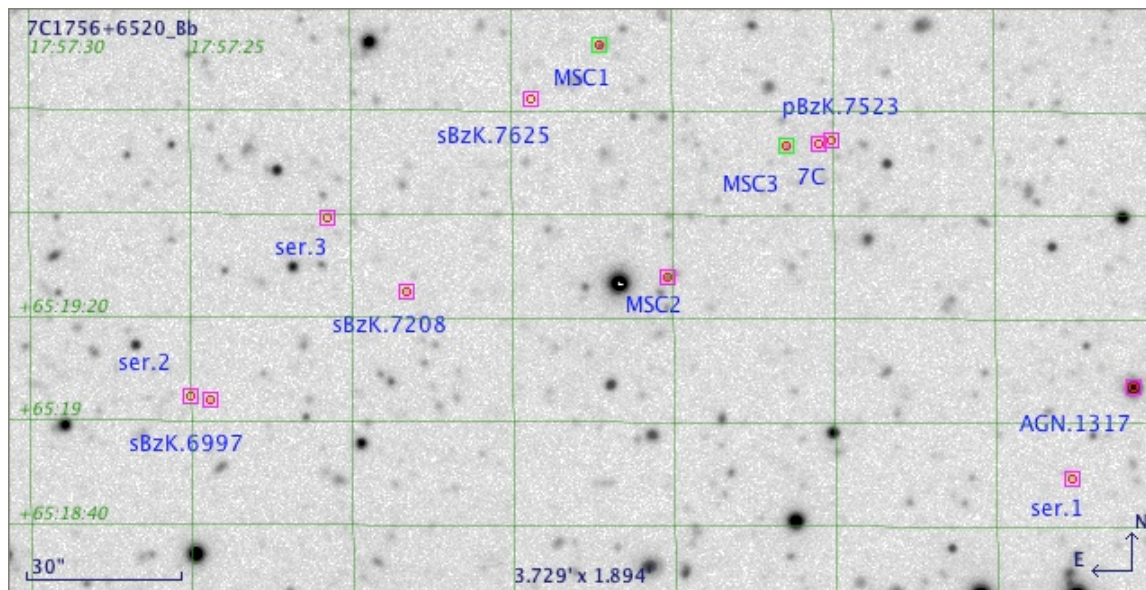


Figure 1. The location of the observed galaxies in the B-band image. North in on the top, East to the left. The field of view is $\sim 3.7' \times \sim 1.9'$.

Table 1. Observed targets: Col. 1 object name, Cols. 2, 3, coordinates(J2000), Col. 4 spectroscopic redshifts from Galametz et al 2010, Col.5 spectroscopic redshifts from this work. We assigned a quality flag A or B to the measured redshifts.

id	R.A. J2000.0	Dec. J2000.0	redshift (G10)	redshift (this work)
serendip.1	17:56:57.67	+65:18:49.45	1.4150±0.0005	1.453 ±0.001 (A)
serendip.2	17:57:25.00	+65:19:04.83	1.4157±0.0010	1.416 (B)
sBzK.6997	17:57:24.43	+65:19:03.87	1.4157±0.0006	1.416 (B)
pBzK.7523 ^a	17:57:05.04	+65:19:54.50	1.4244±0.0004	-
sBzK.7625 ^a	17:57:14.41	+65:20:02.40	1.4366±0.0001	-
sBzK.7208	17:57:18.31	+65:19:24.94	1.4374±0.0002	1.4376±0.0005 (A)
serendip.3	17:57:20.76	+65:19:39.14	1.4379±0.0007	1.4371±0.0005 (A)
AGN.1206 ^a	17:57:13.08	+65:19:08.37	1.4371±0.0002	-
AGN.1317	17:56:55.75	+65:19:07.00	1.4162±0.0005	1.4168±0.0005 (A)
MSC2	17:57:10.16	+65:19:28.09	-	1.4556±0.0005 (A)
MSC1	17:57:12.23	+65:20:12.68	-	1.551±0.001 (A)
MSC3	17:57:06.46	+65:19:53.29	-	2.372±0.001 (A)

(a) no detected emission lines

AGNs, already classified by G10 thanks to several broad band features. We also allocated other slits to galaxies not previously studied, for which we obtained spectroscopic redshifts. In Fig.3 we show with squares the location of the galaxies that were observed spectroscopically. In Table 1 we report the identification name for each galaxy (from G10 when available, otherwise they are identified with the name MSC followed by a number), the J2000.0 R.A. and Dec. coordinates, and the spectroscopic redshifts, from literature (G10) and from the present work, when available.

3.1 Spectroscopic observations

We used MOS mode, obtaining spectroscopy of ten star-forming galaxies in the two main groups of the cluster, (i.e. the galaxy cluster centered on the radio galaxy at redshift

$z=1.4156$, and a compact galaxy sub-group at $z \sim 1.437$, see also Sec. 2): seven spectroscopically confirmed by G10 and three without previous observations; we obtained spectra also for two AGNs. The spectroscopic observations were taken in the H band with slit-width of 1 arcsec aiming to include several metallicity diagnostic lines: $H\alpha$, the nitrogen doublet [NII], and the sulphur doublet [SII]. The grating 210-zJHK, with an appropriate tilt, allowed us to cover a spectral range from 1.48 to 1.67 μm in H band. The tilt was set to have a full spectral coverage in the spectral region of our interest for all slits. The resolving power of 210-zJHK in the H bands is $R=7838$, meaning that the spectral resolution is $\sim 4 \text{ \AA}$ suitable to separate emission lines and sky-lines. We adopted the *nodding* procedure, i.e. observing the object of interest at different positions along the slit. This allowed us to do a proper sky subtraction. The total expo-

sure was 5.1 hr in the H band during the nights of June 25 and 26, 2011. A total of 61 exposure, each of 300 s, were taken. We also obtained observations in the J band during the nights from June 26 to 28, 2011, with 52 exposure of 300 s each. Unfortunately the observations in the J band were obtained under unfavorable weather conditions, with sky partially covered by clouds, and they could not be used for our science purpose. The data were spectroscopically calibrated with a standard star observed during the same nights of the science observations.

3.2 Data reduction

Data reduction was done with the Lucifer Spectroscopic Reduction pipeline which is described for the first time in the present work. More details can be found at <http://lbt-spectro.iasf-milano.inaf.it/lreducerInfo/>. It consists in a set of tasks, based on VIPGI (Scodreggio et al. 2005) recipes, working on Linux systems and written in C and Python.

The preliminary steps of the pipeline workflow concern the creation of master calibration frames: *i)* a bad pixel map was created using dark and flat field frames for each observing run; *ii)* a master dark was produced combining several dark frames; *iii)* a master flat was created averaging a set of spectroscopic flats, and it was used to perform the pixel to pixel correction on the scientific frames. It also allowed to automatically locate slits on the scientific frame. *iv)* an inverse dispersion solution was created starting from calibration arc lamps. *v)* a sensitivity function, as well as telluric absorption correction, were obtained using a telluric star observed close in time and in airmass to the scientific frames.

Once all calibration frames were available, cosmic rays and bad pixels were removed, and dark and flat field corrections were applied, then the spectra were extracted. In this step slit curvatures were removed, slits were extracted and wavelength calibrated. The wavelength calibration *rms* for our frames was lower than 0.2 Å. Sky subtraction, based on the Davies sky subtraction algorithm (Davies 2007), was done on 2D extracted, wavelength calibrated spectra. Further sky subtraction residuals were removed subtracting the median computed along the spatial direction for each spectrum column. Finally, the wavelength and flux calibrated spectra obtained in the different nights were combined together to obtain a stack of 2D sky subtracted spectra. Single spectra were extracted from the 2D stacked frame, using a Horne optimal extraction (Horne 1986). An example of the extracted 2D spectra is shown in Fig.3.2.

Emission-line fluxes were measured with the task SPLIT of IRAF. We derived the redshifts with a gaussian fit of the brightest emission-line for each target, which allowed us to find the central wavelength of the line. The uncertainties on the spectroscopic redshifts are due to the combination of the uncertainty on the fitting and the uncertainty on the wavelength calibration (0.15 Å). Following G10, we assigned a quality flag “A” or “B” to the measured redshifts: “A” indicates a secure z_{spec} based on at least two spectral features (H α and [NII]) “B” indicates high-level confidence in the z_{spec} based on a single spectral feature, usually H α . The observed wavelengths in Å and line fluxes in $\text{erg cm}^{-2} \text{s}^{-1}$ are shown in Table 2, while the z_{spec} are in Table1.

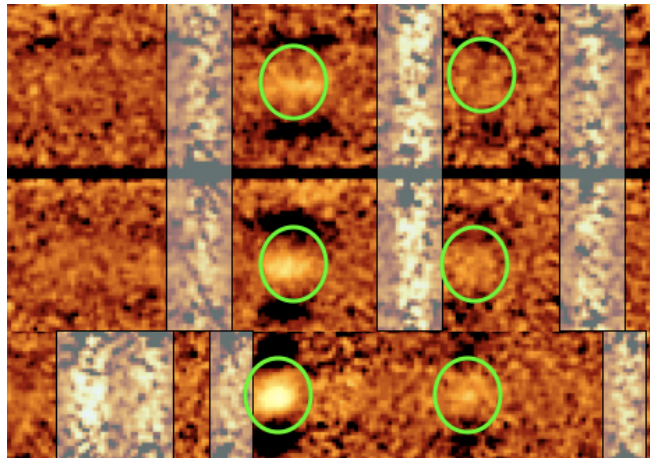


Figure 2. An example of the 2D spectra, namely, from the top, Ser.1, sBzK.7208, and MSC1. The H α and [NII] are shown within (green) circles. The sky emission lines are (grey) shaded. The negative signatures above and below the emission lines are due to the nodding procedure.

4 PARAMETERS OF THE GALAXIES: STELLAR MASS, METALLICITY, AND SFR

The following sections present the methods we adopt to obtain an estimation of the stellar mass, oxygen abundance and star formation rate for the studied galaxies. These derived galaxy parameters are summarized in Table3.

4.1 The stellar masses

We estimated the stellar masses by fitting the multicolour spectral energy distribution (SED), obtained with the observed magnitudes in 5 photometric bands: Palomar-LFC B and z, CFHT/WIRCAM J and K_s , and Spitzer IRAC at 3.6 μm , 4.5 μm . Details of photometric catalogs and data reduction are given in Galametz et al. (2009). For a straightforward comparison with the previous studies on the FMR, we computed the masses with the same procedure described in Cresci et al (2012). The stellar masses were obtained using the code HyperZmass (Pozzetti et al. 2007, 2010) a modified version of the HYPERZ code (Bolzonella et al. 2000) based on the SED fitting technique: for a known spectroscopic redshift we compute the best fitting SED between observed and model fluxes by using the χ^2 minimization. Along with the best fitting SED and its normalization, HyperZmass provides an estimate of the star formation rate, extinction, stellar population age and stellar masses contained in each galaxy, for further details see Cresci et al (2012). We adopted the Bruzual & Charlot (2003) code for spectral synthesis models, using its low resolution version with the Padova 1994 tracks. The models were produced assuming a Chabrier Initial Mass Function (IMF) (Chabrier 2003) with an upper mass limit of $100M_{\odot}$. We have adopted the extinction law of Calzetti et al. (2000) with A_V varying between 0–4 mag, and fixing the redshift to the spectroscopic value. We used smoothly and exponentially decreasing Star Formation Histories (SFHs) with time scale $\tau = [0.1, \infty]$ and age $t = [0.1, 20]$ in Gyr. The stellar masses are reported in Table 3 and an example of our fitting is shown in Fig. 2. The error on the stellar mass is obtained from the SED fitting,

Table 2. Measured emission line fluxes

Galaxy		wavelength (Å)	flux (erg/cm ² s)	FWHM (Å)
Cluster memb.				
serendip.1	H α	16101.31	6.9e-17	21.
	[NII]	16149.52	1.7e-17	5.
sBzK.7208	H α	15998.00	1.0e-16	17.
	[NII]	16052.07	1.8e-17	5.
serendip.3	H α	15994.92	1.2e-16	10.
	[NII]	16046.28	4.0e-17	10.
MSC2	H α	16116.03	1.8e-17	10.
	[NII]	16167.00	<6e-18 ^a	
serendip.2	H α	15860	<4e-18 ^a	
sBzK.6997	H α	15860	<4e-18 ^a	
AGN.1317				
	H β b	11724.85	non cal.	78.
	[OIII]	11978.53	non cal.	9.
	[OIII] b	11968.86	non cal.	24.
	[OIII]	12094.50	non cal.	9.
	[OIII] b	12084.83	non cal.	24.
	H α	15861.04	2.8e-16	9.
	[NII]	15812.72	5.2e-17	9.
	[NII]	15906.94	9.3e-17	9.
	H α b	15851.38	9.7e-16	121.
	[SII]	16228.27	4.4e-17	9.
	[SII]	16264.51	2.0e-17	9.
non memb.				
MSC1	H α	16743.2	1.9e-16	8.
	[NII]	16796.2	4.9E-17	10.
MSC3	[OII]	12572.77	non cal.	11.
	[OIII]	16883.93	1.2E-16	10.

(a) upper limit obtained measuring the continuum flux in the same spectral region where the emission line is expected

while the uncertainty on A_V is the formal error due to the step in extinction adopted by HYPERZ. The latter errors are indeed lower limit on the uncertainty on the extinction. The major source of error is due to adopt a value of A_V obtained from SED fitting, thus valid for the stellar component, also to the gaseous component. It is known that dust extinction for nebular lines could be larger by a factor of ~ 2 (e.g., Calzetti et al. 2000). Although this effect is still uncertain at high redshift, recently Förster Schreiber et al. (2009) suggest that the H α based SFRs, with extra dust attenuation by a factor of ~ 2 , are in good agreement with those derived from the SED fitting for their SINS galaxies at $z \sim 2$, consistently with the results by Calzetti et al. (2000). Logarithm of the stellar masses ranges between 9.8 and 10.5 indicating that we are observing the most massive star-forming galaxies in the cluster, missing the fainter population of less massive and dwarf galaxies.

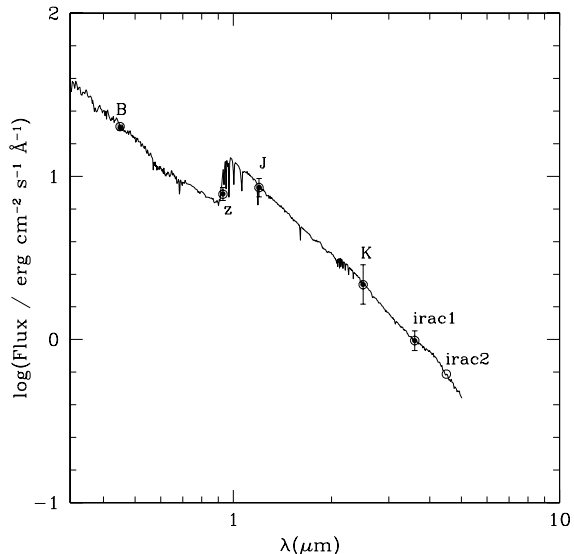


Figure 3. An example of our SED fitting for the galaxy MSC 2: the continuous line is the best fitting, the filled circles are the measured fluxes, and the empty circles are the fluxes expected on the basis of the best fitting.

4.2 Metallicity determination

We used $N2 = [NII]/H\alpha$ ratio to infer the metallicity of the galaxies using the calibrations obtained by Nagao et al. (2006) and Maiolino et al. (2008). The wavelength separation between the two lines is very small and thus this ratio is not affected by the extinction effects. The uncertainties of the gas-phase metallicities, of the order of 0.1-0.2 dex result from both the error on the calibration itself and the error on the estimation of [NII] emission line (that can reach 50-70%, while typical error on the H α fluxes are 10%). Even if N2 is commonly adopted as a metallicity indicator, it is necessary to remember the intrinsic limit of the metallicity measurement with N2 which depends not only on O/H, but also on N/O. The relation between N2 and $12 + \log(O/H)$ is based on the observations of star-forming galaxies or single HII regions in the Local Universe. The relation is not linear: at low oxygen abundances the primary production of nitrogen dominates (N/O is constant), at high oxygen abundance the secondary production of nitrogen dominates (N/O increases with $12 + \log(O/H)$). The observed relation has however a large scatter since N/O ratio is also a clock of the last major episode of star formation (e.g., van Zee et al. 1998). Low values of N/O might not only imply low metallicity, but they might be the signature of a very recent burst of star formation, while high values of N/O might also imply galaxies with a long quiescent period. This effect is more dominant in dwarf galaxies whose SF is characterized by bursty episodes, while massive galaxies have a more continuous star formation history (see also Pérez-Montero & Contini 2009; Zahid et al. 2012; Maiolino et al. 2012).

4.3 The Star Formation Rate

We have derived the SFR from the $H\alpha$ flux, which provides a direct probe of the young massive stellar population. We have used the relationship given by Kennicutt (1998), and scaled down the results by a factor of 1.7 (Pozzetti et al. 2007) to convert them to the Chabrier (2003) IMF, as described by Cresci et al (2012). The conversion factor is based on the $H\alpha$ flux corrected for dust extinction. Thus a good knowledge of the amount of extinction which affects the emission lines is required. Since we were not able to measure the Balmer ratio $H\alpha/H\beta$, from which the extinction can be derived, we have used the extinction A_V derived from the SED fitting described in Sec.4.1. The errors on the SFR take into account the error on the $H\alpha$ flux ($\sim 10\%$) and the formal error in the extinction (0.2 mag). Consistently with what discussed in Sec.4.1, we have also computed the SFRs using A_V value multiplied by a factor 2, which seem to be more appropriate for the gaseous component (Förster Schreiber et al. 2009). In Tab.3 we present the SFR values obtained with A_V from SED fitting, while in Fig.4 (right panel) we show both values of $\mu = \log M - \alpha \log \text{SFR}$, obtained with the SFR corrected with nebular (empty circles) and stellar (filled circles) A_V .

5 THE MASS-METALLICITY AND THE FUNDAMENTAL METALLICITY RELATIONS

In the Local Universe, there is not an unanimous agreement on the effect of cluster membership in the chemical evolution of galaxies. Ellison et al. (2009) presented data for 1318 galaxies in local clusters, obtaining their stellar mass and gas-phase abundances. By comparing the MZR of the cluster galaxies with a control sample of galaxies matched in mass and redshift, they found that cluster galaxies have, on average, at a given mass higher metallicities by up to 0.04 dex. However they found that this effect is not related simply to cluster membership, nor to cluster properties. They attributed it to local scale processes, such as the presence of a close companion or several near neighbours that lead to an enhanced metallicity. On the other hand, Petropoulou et al. (2012) from the detailed analysis of dwarf galaxies four nearby clusters, have found that the enhancement of the gas-phase metallicity is sensitive to the cluster mass, and appears to be more prominent in the inner regions of massive clusters. They claim that this evidence points towards a possible connection of the chemical enrichment of cluster galaxies with their ICM properties. To clarify these aspects we are planning to present an analysis of the effect of the environment on the FMR in galaxies in nearby clusters in a forthcoming paper.

In the high-redshift Universe, the situation is even less defined due to the limited number of works dedicated to this issue. Most of the works dedicated to clusters at $z > 1$ focussed their attention on the spatial distribution of star-forming and non-star-forming galaxies. Hayashi et al. (2011) analyzed a sample of star-forming galaxies at $z=1.46$ and they found that the galaxies located close to the cluster core are experiencing high star-forming activity comparable to those in other lower-density regions. Fassbender et al.

(2009) also found an on-going starburst activity in a cluster at $z=1.56$, and from a comparison with literature data they concluded that most of the clusters at $z \sim 1.5$ are likely to hold active star formation in the core regions. On the contrary, in other clusters with slightly lower redshifts the star formation activity has been found significantly weaker than that in the surrounding regions (at $z=0.8$ and $z=1.39$, Lidman et al. 2008; Koyama et al. 2010; Bauer et al. 2011).

To our knowledge, only Hayashi et al. (2011) have intended to investigate the metallicity in a cluster at $z > 1$ observing several star-forming galaxies in the cluster XMMXCSJ2215.9-1738 at $z=1.46$. Their results suggest that the metallicity in that cluster is not (yet) strongly dependent on environment and that the cluster galaxies are located on a MZR, similarly to that of the star-forming galaxies in the field at $z \sim 2$. However, due to non-photometric weather conditions, Hayashi et al. (2011) were not able to calibrate their $H\alpha$ flux and thus a direct comparison with our SFRs is not feasible.

With our observations of the cluster 7C 1756+6520 we are adding another piece of information to the view of the evolution of galaxies within a cluster by having the complete information of the stellar masses, SFR, and metallicity. Mannucci et al. (2010) have shown that it exists a combination of the stellar mass and SFR which better correlates with the metallicity. In Fig.4 we show in the left panel the *classical* MZR and its evolution with redshift and in the right panel the projection of the FMR in the plane $\log M - \alpha \log \text{SFR}$, where $\alpha = 0.32$. The shaded area represent the local SDSS galaxies at $z \sim 0.1$ (see Mannucci et al. (2010)). We note immediately an evolution of the MZR relation with the redshift: the galaxies of the cluster at $z \sim 1.4$ do not follow to local MZR, having at a given mass a lower metallicity. The MZR of the cluster is indeed in between the MZR derived by Cresci et al (2012) at $z \sim 0.63$ and by Erb (2008) at $z \sim 2.2$.

When we apply to the MZR the correction for the SFR, we found that the galaxies of the cluster lie in the locus of the Local Universe galaxies, the so-called FMR which is valid for field galaxies up to $z \sim 2.5$. Note that in the plot we have also included the galaxy MSC 1 (in magenta), which has a redshift of 1.55, thus clearly outside the cluster. The galaxies belonging to the two sub-groups of the cluster 7C 1756+6520 (filled red circles) are in good agreement with the FMR derived from isolated galaxies. This is also true when a the nebular extinction (two times the extinction derived from SED fitting) is applied. This affect marginally the value of μ for the galaxies with a higher extinction (empty circles in Fig.4).

Is this absence of deviation expected? or is it telling us something new about the evolution of galaxies in cluster in the early phases of their evolution? In Fig.5 we show the metallicity difference from the FMR (defined with SDSS galaxies at $z \sim 0.1$) for galaxies at different redshifts. For field galaxies the result of Mannucci et al. (2010) is that all galaxies up to $z=2.5$ are consistent with no evolution of the FMR. Our observations, even if affected by a small statistics, suggest that star-forming galaxies in clusters at $z \sim 1.4$ follow the FMR in the same way as field galaxies¹. As shown in Fig. 4 the av-

¹ The average has been computed without including the upper limit value

Table 3. Galaxy properties

id	B	z	J	K	IRAC3.6	IRAC4.5	$\log(M_{\text{star}})$	$12+\log(\frac{O}{H})$	$\log(\text{SFR})$	A_V
ser.1	23.06 ± 0.06	23.11 ± 0.13	22.16 ± 0.13	21.02 ± 0.14	—	21.12 ± 0.14	10.4 ± 0.15	8.82 ± 0.12	0.7 ± 0.2	0.2 ± 0.2
sBzK.7208	24.93 ± 0.07	23.46 ± 0.14	22.00 ± 0.22	—	21.29 ± 0.06	21.33 ± 0.11	10.0 ± 0.2	8.70 ± 0.12	1.4 ± 0.2	1.9 ± 0.2
ser.3	25.29 ± 0.11	23.18 ± 0.14	21.50 ± 0.15	—	21.27 ± 0.05	21.77 ± 0.15	10.5 ± 0.15	8.96 ± 0.14	0.9 ± 0.2	0.0 ± 0.2
MSC1	23.57 ± 0.04	21.71 ± 0.10	21.68 ± 0.14	22.87 ± 0.30	22.54 ± 0.15	—	9.8 ± 0.2	8.62 ± 0.14	1.5 ± 0.2	0.0 ± 0.2
MSC2	23.58 ± 0.04	22.72 ± 0.11	22.66 ± 0.16	—	—	—	9.8 ± 0.2	$< 8.92^a$	0.03 ± 0.2	1.1 ± 0.2

(a) upper limit on [NII] measurement

erage difference of our galaxy metallicity with the FMR is very small. Our results indicate that, in high redshift clusters, the chemical evolution is driven by the intrinsic *nature* of the galaxy evolution, and that external perturbations are not observable in terms of location of galaxies in the FMR. However, the uncertainties on our metallicity measurements prevent us to estimate differences of the order of 0.04 dex, as observed by Ellison et al. (2009) between cluster and field galaxies. A comparison with the FMR in the Local Universe clusters is necessary, and will be the argument of a forthcoming paper.

A possible explanation to this lack of effects due to cluster membership is the large extension of the structure around the radio galaxy 7C 1756+6520 and in high- z clusters in general. The cosmological simulation of Poggianti et al. (2010) found that the number of galaxies in cluster per unit volume is higher by approximately a factor of 4.7 at $z=1.5$, compared to $z=0$. They also found that the most massive and the least massive clusters or groups are on average equally dense, at a given redshift. However, these considerations apply to virialized regions, and probably are not valid in the case of large scale structure as that around 7C 1756+6520. Often over-densities at the highest redshifts have a filamentary nature and extend beyond ~ 2 Mpc (Croft et al. 2005; Zappacosta et al. 2002; Mannucci et al. 2007). As described by G10, 7C 1756+6520 is part of a large scale galaxy structure composed of (at least) two main groups - a galaxy cluster centered on the radio galaxy at $z=1.4156$ and a compact group at $z \sim 1.437$, $1.5'$ east of the radio galaxy. In this filamentary structure the influence of galaxy interaction or of the ICM has not modified the galaxy evolution enough to change their position in the FMR plane. Observations of the X-ray emission of the ICM of this cluster would be extremely useful to study its dynamical state.

6 THE BRIGHT AGN 1317

Seven AGNs, including the central radio galaxy, have been spectroscopically confirmed in close proximity both spatially and in redshift space of the cluster. Three of them are found within $1.5'$ of the radio galaxy, including AGN.1317. We present the spectroscopic observations of AGN.1317 both in J and H bands. As mentioned in Section 3.1, it was not possible to perform a proper flux calibration of the J-band data. To obtain a rough calibration, we re-scaled the J-band data to match the H-band continuum by a simple visual comparison of the two spectral bands. The spectrum of AGN.1317 (Fig. 6) shows clear broad features,

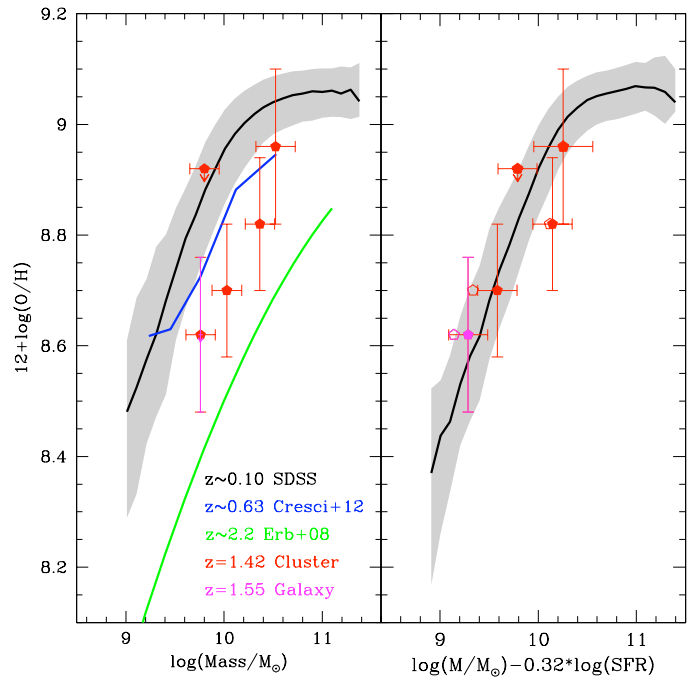


Figure 4. The FMR in the cluster 7C 1756+6520: left panel, the MZR as defined by the SDSS galaxies at $z\sim 0.1$ (black curves, and shaded area), at $z\sim 0.63$ (blue curve), and at $z\sim 2.2$ (green curve); right panel, the projection of the FMR in the plane $\mu = \log M - \alpha \log \text{SFR}$, where $\alpha = 0.32$. In both panels red filled circles are the galaxies observed in the cluster 7C 1756+6520, while the magenta filled circle is the galaxy projected on the cluster area with a redshift $z=1.55$ (SFR computed with the extinction from SED fitting). The empty circles show the μ values obtained with the SFR with the nebular extinction.

as $H\beta(\text{FWHM} = 4800 \pm 500 \text{ km/s})$ and $H\alpha(\text{FWHM} = 5520 \pm 250 \text{ km/s})$, associated with the broad line region (BLR), and forbidden lines primarily associated with the AGN narrow line region (NLR): the [OIII], [NII] and [SII] doublets.

The [OIII] $\lambda\lambda 4959, 5007$ lines show a clear asymmetric profile with prominent blue-shifted wings. This is a characteristic signature of outflow. In fact, as observed in local AGN (Müller-Sánchez et al. 2011), the net outflow of the NLR clouds through a dusty region (of the host galaxy) implies that the emission from the clouds on the far, red-shifted

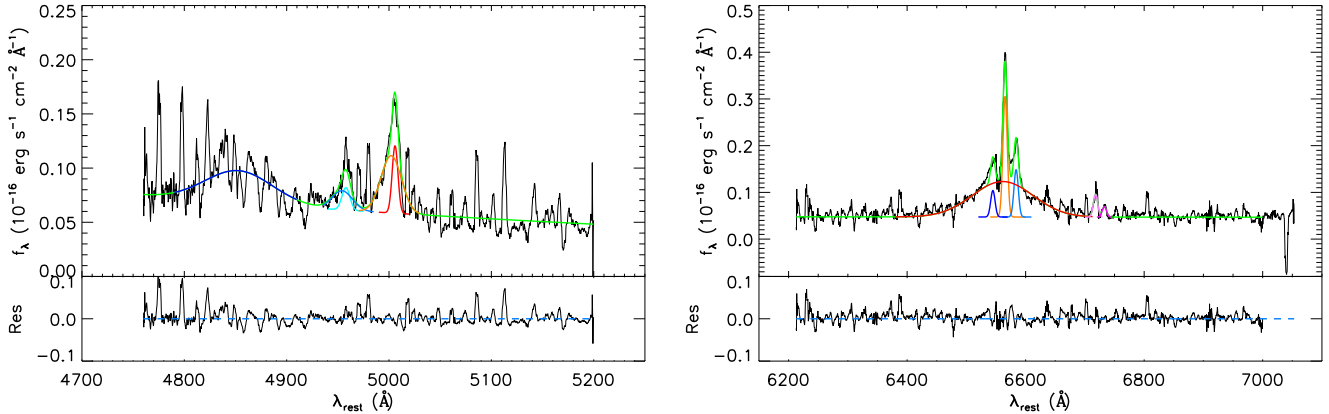


Figure 6. AGN. 1317 rest frame spectrum. *Left:* J-band data, normalized to match the H-band continuum. *Right:* H-band data. In both panels, the green line represents the global fit to the data with residuals shown in the bottom board. The reduced χ^2 are 1.7 for the J-band and 1.3 for the H-band fitting. Emission features are fitted by Gaussian shapes. In the *left* panel, dark blue is for the $H\beta$ (4861Å), sky blue and cyan for the $[OIII]\lambda 4959$ (narrow and broad components, respectively), orange and red for the the $[OIII]\lambda 5007$ (narrow and broad components, respectively). In the *right* panel, red and orange for the $H\alpha$ (6563Å, broad and narrow components, respectively), blue and sky blue for the $[NII]$ lines (6548Å and 6584Å, respectively), while light and dark pink are respectively for the $[SII]\lambda 6716\text{Å}, \lambda 6731\text{Å}$.

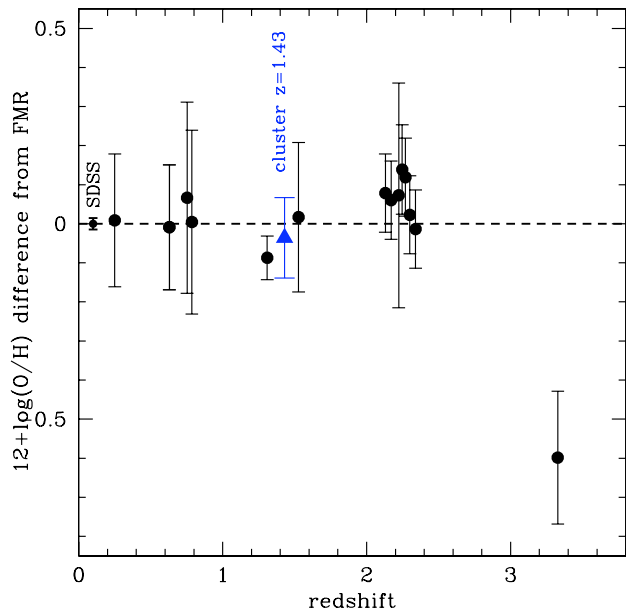


Figure 5. The metallicity difference from the FMR (defined with SDSS galaxies at $z\sim 0.1$) for galaxies at different redshifts. For field galaxies the results of Mannucci et al. (2010) is that all galaxies up to $z=2.5$ are consistent with no evolution of the FMR. The filled circles are from Mannucci et al. (2010), the filled triangle is the result of the present work.

side is suppressed relative to the emission on the near, blue-shifted side.

The $[OIII]\lambda\lambda 4959, 5007$ lines are well fitted by two Gaussians (narrow and blue-shifted components) as seen in Fig 6. The gaussians of the doublet of narrow lines are forced to have the theoretical intensity ratio (i.e. $[OIII]\lambda 4959/[OIII]\lambda 5007=1/3$), the same FWHMs, and their known rest-frame wavelengths. The blue-shifted components are treated in a similar way, but we allow the central wavelengths to vary. This yields a FWHM ~ 550 km/s for the narrow components, nicely consistent with typical NLR values. The asymmetric wings are reproduced by broader Gaussians (FWHM ~ 1420 km/s) blue-shifted by 430 ± 180 km/s. These FWHMs are much broader than usually found in the NLR of local AGNs (Müller-Sánchez et al. 2011) and are rather consistent with what observed in powerful quasars at higher redshift (Cano-Díaz et al. 2012). The $[OIII]$ doublet primarily traces the gas in the NLR ionized by the AGN, thus the most probable explanation is that the strong outflow might be driven by the AGN radiation pressure itself. The origin of the wind from the AGN is also supported by the huge velocities (the out-flowing gas reaches an excess of 1000 km/s) which cannot be explained by supernovae-driven outflows (Nath & Silk 2009). This is the first time that such powerful AGN-driven winds are detected in source located at the edges of a high redshift cluster (the projected distance between the central radio galaxy and AGN. 1317 being ~ 780 kpc). Indeed, at $z > 1$ AGN outflows traced by $[OIII]$ emission have been detected only in isolated sources so far (Nesvadba et al. 2008, 2011; Alexander et al. 2010). However, to draw some conclusion about the significance of this outflow (i.e. the out-flowing mass, at which rate, whether the outflow can affect the cluster environment, etc.), it is necessary a follow-up with calibrated J-band data.

7 CONCLUSIONS

We have presented new infrared spectroscopic observations with LUCIFER@LBT of a sample of star-forming galaxies in the two main sub-groups of the cluster associated with the radio galaxy 7C1756+6520. With available photometric data and with our spectroscopic information, we have derived their stellar mass, metallicity and SFR. We have then located them in the MZ plane and in the FMR. The galaxies in the $z \sim 1.4$ cluster are perfectly consistent with the FMR, suggesting that the effect of the environment is not dominant in the early phases of their evolution. Finally, we have detected in the [OIII] doublet a strong gas outflow reaching velocities > 1000 km/s that is possibly driven by the AGN radiation pressure. This source, AGN. 1317, is located at the edges of the cluster and further observations are required to study the effect of such strong wind on both the host and cluster environments.

ACKNOWLEDGMENTS

L. Magrini and E. Sani acknowledge financial support from ASI under Grant I/009/10/0/.

REFERENCES

- Ageorges, N., Seifert, W., Jutte, M., et al., 2010, SPIE, 7735, 53
- Alexander D. M., Swinbank A. M., Smail I., McDermid R., Nesvadba N. P. H., 2010, MNRAS, 402, 2211
- Arnaud, M., 2009, A&A, 500, 103
- Bauer, A. E., Grützbauch, R., Jørgensen, I., Varela, J., & Bergmann, M. 2011, MNRAS, 411, 2009
- Blakeslee, J. P., Franx, M., Postman, M., et al. 2003, ApJL, 596, L143
- Bolzonella, M., Kova, K., Pozzetti, L., et al., 2010, A&A, 524, 76
- Bolzonella, M., Miralles, J.-M., & Pelló, R. 2000, A&A, 363, 476
- Bruzual, G., & Charlot, S., 2003, MNRAS, 344, 1000
- Calzetti, D., Armus, L., Bohlin, R. C., et al., 2000, ApJ, 533, 682
- Campisi, M. A., Tapparello, C., Salvaterra, R., et al., 2011, MNRAS, 1437
- Cano-Díaz M., Maiolino R., Marconi A., Netzer H., Shemmer O., Cresci G., 2012, A&A, 537, L8
- Cresci, G., Mannucci, F., Sommariva, V., et al, 2012, MNRAS, tmp.2212
- Croft, S., Kurk, J., van Breugel, W., et al., 2005, AJ, 130, 867
- Chabrier, G., 2003, ApJ, 586, 133
- Chung, A., van Gorkom, J. H., Kenney, J. D. P., Crowl, H., & Vollmer, B. 2009, AJ, 138, 1741
- Daddi, E., Cimatti, A., Renzini, A., et al., 2004, ApJ, 617, 746
- Davé, R., Finlator, K., Oppenheimer, B. D., 2011, MNRAS, 416, 135
- Davies, R. I. 2007, MNRAS, 375, 1099
- Dayal, P., Ferrara, A., & Dunlop, J. S. 2012, arXiv:1202.4770
- di Serego Alighieri, S., Vernet, J., Cimatti, A., et al. 2005, A&A, 442, 125
- Dressler, A., 1980, ApJ, 236, 351
- Ellison, S. L., Simard, L., Cowan, N. B., et al., 2009, MNRAS, 397, 467
- Erb, D. K., Steidel, C. C., Shapley, A. E., et al., 2006, ApJ, 646, 107
- Erb, D. K. 2008, ApJ, 674, 151
- Eisenhardt, P. R. M., Brodwin, M., Gonzalez, A. H., et al. 2008, ApJ, 684, 905
- Fassbender, R., Nastasi, A., Boehringer, H., et al., 2011, A&A, 527, 10
- Finlator, K., & Davé, R., 2008, MNRAS, 385, 2181
- Finn, R. A., Zaritsky, D., McCarthy, D. W., Jr., et al., 2005, ApJ, 630, 206
- Förster Schreiber, N. M., Genzel, R., Bouché, N., et al. 2009, ApJ, 706, 1364
- Galametz, A., De Breuck, C., Vernet, J., et al. 2009, A&A, 507, 131 (G09)
- Galametz, A., Stern, D., Stanford, S. A., et al. 2010, A&A, 516, A101 (G10)
- Galametz, A., Vernet, J., De Breuck, C., et al. 2010, A&A, 522, A58
- Gobat, R., Daddi, E., Onodera, M., et al. 2011, A&A, 526, A133
- Hayashi, M., Kodama, T., Koyama, Y., et al., 2011, MNRAS, 415, 2670
- Hatch, N. A., De Breuck, C., Galametz, A., et al. 2011, MNRAS, 410, 1537
- Hill, J. M., Green, R. F., & Slagle, J. H., 2006, SPIE, 6267, 31
- Hilton, M., Collins, C. A., Stanford, S. A., et al. 2007, ApJ, 670, 1000
- Hilton, M., Stanford, S. A., Stott, J. P., et al., 2009, 697, 436
- Horne, K. 1986, PASP, 98, 609
- Kennicutt, R. C., Jr. 1998, ARA&A, 36, 189
- Koyama, Y., Kodama, T., Shimasaku, K., et al., 2010, MNRAS, 403, 1611
- Kuiper, E., Hatch, N. A., Venemans, B. P., et al. 2011, MNRAS, 417, 1088
- Lequeux, J., Peimbert, M., Rayo, J. F., et al., 1979, A&A, 80, 155
- Lidman, C., Rosati, P., Tanaka, M., et al. 2008, A&A, 489, 981
- Maiolino, R., Nagao, T., Grazian, A., et al., 2008, A&A, 488, 463
- Maiolino, R. et al., 2012, in prep.
- Mannucci, F., Bonoli, G., Zappacosta, L., Maiolino, R., & Pedani, M. 2007, A&A, 468, 807
- Mannucci, F., Cresci, G., Maiolino, R., et al., 2009, MNRAS, 398, 1915
- Mannucci, F., Cresci, G., Maiolino, R., et al., 2010, MNRAS, 408, 2115
- Mannucci, F., Salvaterra, R., & Campisi, M. A., 2011, MNRAS, 414, 1263
- Müller-Sánchez F., Prieto M. A., Hicks E. K. S., Vives-Arias H., Davies R. I., Malkan M., Tacconi L. J., Genzel R., 2011, ApJ, 739, 69
- Nagao, T., Maiolino, R., & Marconi, A., 2006, A&A, 459, 85
- Nakata, F., Kodama, T., Shimasaku, K., et al., 2005, MN-

- RAS, 357, 1357
- Nath B. B., Silk J., 2009, MNRAS, 396, L90
- Nesvadba N. P. H., Lehnert M. D., De Breuck C., Gilbert A. M., van Breugel W., 2008, A&A, 491, 407
- Nesvadba N. P. H., Polletta M., Lehnert M. D., Bergeron J., De Breuck C., Lagache G., Omont A., 2011, MNRAS, 415, 2359
- Papovich, C. 2008, ApJ, 676, 206
- Papovich, C., Momcheva, I., Willmer, C. N. A., et al. 2010, ApJ, 716, 1503
- Pérez-Montero E., Contini T., 2009, MNRAS, 398, 949
- Petropoulou, V., Vilchez, J. M., & Iglesias-Paramo, J. 2012, arXiv:1202.4164
- Poggianti, B. M., von der Linden, A., De Lucia, G., et al., 2006, ApJ, 642, 188
- Poggianti, B. M., De Lucia, G., Varela, J., et al., 2010, MNRAS, 405, 995
- Pozzetti, L., Bolzonella, M., Lamareille, F., et al., 2007, A&A, 474, 443
- Pozzetti, L., Bolzonella, M., Zucca, E., et al., 2010, A&A, 523, 13
- Rosati, P., Tozzi, P., Ettori, S., et al., 2004, AJ, 127, 230
- Rosati, P., Tozzi, P., Gobat, R., et al., 2009, A&A, 508, 583
- Scodeggio, M., Franzetti, P., Garilli, B., et al. 2005, PASP, 117, 1284
- Seifert, W., Ageorges, N., Lehmitz, M., et al., SPIE, 7735, 256
- Sommariva, V., Mannucci, F., Cresci, G., et al. 2011, A&A, 539, A136
- Stanford, S. A., Eisenhardt, P. R., Brodwin, M., et al., 2005, ApJ, 634, 129
- Stanford, S. A., Romer, A. K., Sabirli, K., et al., 2006, ApJ, 646, 13
- Tanaka, M., Lidman, C., Bower, R. G., et al., 2009, A&A, 507, 671
- Tanaka, M., De Breuck, C., Venemans, B., et al, 2010, A&A, 518, 18
- Tremonti, C. A., Heckman, T. M., Kauffmann, G., et al. 2004, ApJ, 613, 898
- van Zee, L., Salzer, J. J., & Haynes, M. P. 1998, ApJL, 497, L1
- Venemans, B. P., Röttgering, H. J. A., Miley, G. K., et al. 2007, A&A, 461, 823
- Wilson, G., Muzzin, A., Yee, H. K. C., et al. 2009, ApJ, 698, 1943
- Zahid, H. J., Bresolin, F., Kewley, L. J., Coil, A. L., & Davé, R. 2012, arXiv:1203.0558
- Zappacosta, L., Mannucci, F., Maiolino, R., et al. 2002, A&A, 394, 7